9-1-2010

Compact binaries in star clusters - I. Black hole binaries inside globular clusters

J. M.B. Downing

M. J. Benacquista

M. Giersz

R. Spurzem

Recommended Citation

J. M.B. Downing, et. al., (2010) Compact binaries in star clusters - I. Black hole binaries inside globular clusters.Monthly Notices of the Royal Astronomical Society407:31946. DOI: http://doi.org/10.1111/j.1365-2966.2010.17040.x

Monthly Notices
of the
ROYAL ASTRONOMICAL SOCIETY

Mon. Not. R. Astron. Soc. **407,** 1946–1962 (2010) doi:10.1111/j.1365-2966.2010.17040.x

Compact binaries in star clusters – I. Black hole binaries inside globular clusters

J. M. B. Downing,[1⋆†] M. J. Benacquista,[2] M. Giersz[3] and R. Spurzem[1,4,5]

[1]*Astronomisches Rechen-Institut, Zentrum für Astronomie der Universität Heidelberg, Mönchhofstraße 12-14, D-69120 Heidelberg, Germany*
[2]*Center for Gravitational Wave Astronomy, University of Texas at Brownsville, Brownsville, TX 78520, USA*
[3]*Nicolaus Copernicus Astronomical Center, Polish Academy of Sciences, ul. Bartycka 18, 00-716 Warsaw, Poland*
[4]*National Astronomical Observatories, Chinese Academy of Sciences, 20A Datun Rd, Chaoyang District 100012, China*
[5]*Kavli Institute of Astronomy and Astrophysics, Peking University, Beijing 100871, China*

Accepted 2010 May 18. Received 2010 April 5; in original form 2009 October 3

ABSTRACT

We study the compact binary population in star clusters, focusing on binaries containing black holes, using a self-consistent Monte Carlo treatment of dynamics and full stellar evolution. We find that the black holes experience strong mass segregation and become centrally concentrated. In the core the black holes interact strongly with each other and black hole–black hole binaries are formed very efficiently. The strong interactions, however, also destroy or eject the black hole–black hole binaries. We find no black hole–black hole mergers within our simulations but produce many hard escapers that will merge in the Galactic field within a Hubble time. We also find several highly eccentric black hole–black hole binaries that are potential Laser Interferometer Space Antenna (LISA) sources, suggesting that star clusters are interesting targets for space-based detectors. We conclude that star clusters must be taken into account when predicting compact binary population statistics.

Key words: gravitational waves – binaries: close – globular clusters: general.

1 INTRODUCTION

The inspirals and mergers of compact binaries where both members are neutron stars (NSs) or black holes (BHs) are some of the most promising sources for the current and next generation of ground-based gravitational wave (GW) detectors (LIGO, Virgo, GEO 600, TAMA 300). NS–NS binaries are expected to be the most plentiful merger species in the frequency regime of ground-based detectors (Abbott et al. 2005; Belczynski et al. 2007), however, BH–BH binaries are more massive and thus can be detected at larger distances, as far as the Virgo cluster (Abbott et al. 2006) for the current generation of GW detectors and up to cosmological distances for the next generation. Compact binaries with longer periods and including white dwarfs (WDs) may also be detectable in the low-frequency (5×10^{-5}–1 Hz) Laser Interferometer Space Antenna (LISA) frequency band (Hils, Bender & Webbink 1990; Benacquista 2001; Nelemans, Yungelson & Portegies Zwart 2001; Belczynski, Benacquista & Bulik 2008). WD–WD binaries will be the most plentiful stellar mass LISA sources and are expected to produce confusion limited noise (e.g. Evans, Iben & Smarr 1987; Hils et al. 1990; Nelemans et al. 2001; Timpano, Rubbo & Cornish 2006; Ruiter et al. 2007) whereas the less common NS–NS, NS–BH and BH–BH binaries are potentially resolvable.

In order to make predictions for GW event rates, the population of compact binaries in the Universe must be understood. While the population of NSs in the local Universe can be constrained by observations of pulsars (e.g. Kalogera et al. 2001; Lorimer 2005), BHs cannot be observed directly and their properties can only be constrained by modelling. There have been several studies carried out on the compact binary population in the galactic field where stellar and binary evolution proceeds in isolation and can be modelled using simple population synthesis. In particular Belczynski et al. (2007) predict a detection rate for the advanced LIGO detector of ∼20 NS–NS mergers yr^{-1}, only ∼2 BH–BH mergers yr^{-1} and ∼1 NS–BH merger yr^{-1}. Thus the detection rate in the galactic field should be dominated by NS–NS mergers. Belczynski et al. (2008) have performed similar calculations for the galactic field in the LISA band. Depending upon the assumptions made about the probability of mergers during common envelope evolution they find two–six resolvable NS–NS binaries and zero–five resolvable BH–BH binaries. This implies that, although rare, both NS–NS and BH–BH binaries may appear as resolved stellar mass sources in the LISA band. Overall NS–NS binaries will dominate the field detection rate for ground-based detectors while a detection in the LISA band is possible but unlikely.

⋆E-mail: downin@ari.uni-heidelberg.de
†Fellow of the International Max-Planck Research School for Astronomy and Cosmic Physics at the University of Heidelberg, Heidelberg, Germany.

In star clusters the situation is rather different. Here interactions between stars and binaries are common (e.g. Heggie 1975) and can affect the final outcome of binary evolution. Such interactions can form new binaries from single stars, exchange binary members and field stars and can reduce or increase the period of existing binaries. In order to maintain energy equipartition, interactions between particles of different masses tend to accelerate the lowest mass particles to the highest velocities (Spitzer 1987). As a consequence low-mass objects are the most likely to escape during few-body encounters. Therefore few-body interactions tend to introduce massive objects into binaries. Massive objects also tend to sink to the centre of star clusters where the stellar density is highest (mass segregation, also a consequence of energy equipartition; Spitzer 1987) and thus massive objects are the most likely to experience dynamical interactions. Since BHs rapidly become the most massive objects in star clusters due to stellar evolution they will be particularly strongly affected by dense stellar environments and are very likely to be exchanged into binaries. Therefore star clusters are predicted to form BH–BH binaries rather efficiently (Sigurdsson & Phinney 1993) and may significantly enhance the BH–BH merger rate in the Universe.

Several authors have investigated this possibility using various approximations. Gültekin, Miller & Hamilton (2004) and O'Leary et al. (2006) have simulated the formation of intermediate-mass black holes (IMBHs) assuming that the BHs in the cluster are completely mass segregated and interact only with each other. In this situation, where the BHs interact very strongly, the authors resolve these encounters with explicit few-body integration. The interactions can lead to the efficient formation of BH–BH binaries but also tend to destroy or eject those already formed. These authors conclude that GW mergers can occur within young star clusters but BH–BH binaries will be destroyed rather efficiently and the population will be depleted within a few Gyrs. O'Leary et al. (2006) in particular calculate a star cluster BH–BH detection rate for advanced LIGO of 1–10 mergers yr^{-1}, up to 70 per cent of which actually occur in ejected BH–BH binaries and thus take place in the galactic field. Neither set of authors includes stellar evolution in their simulations. By contrast Ivanova et al. (2008) and Sadowski et al. (2008) have conducted studies of the compact binary population in star clusters using stellar evolution prescriptions and simplified two-zone models of cluster dynamics. The two-zone models assume that the BHs and BH–BH binaries remain in dynamical equilibrium with the rest of the cluster and do not strongly mass segregate. Thus the density of BHs and BH–BH binaries remains low and they do not interact with each other nearly as frequently as in the previous models. Sadowski et al. (2008) in particular find no NS–NS mergers but a much higher rate of BH–BH mergers than O'Leary et al. (2006). They calculate a detection rate of 25–3000 mergers yr^{-1} for advanced LIGO even though their treatment of the few-body interactions is the same as for O'Leary et al. (2006). This is because although there are fewer interactions that create BH–BH binaries there are also fewer interactions that destroy them. This highlights the importance assumptions about global cluster dynamics can have on detection rates. The only study with full treatment of both dynamics and stellar evolution is that of Portegies Zwart & McMillan (2000) who conducted small ($N \sim$ a few 10^3) direct N-body simulations and showed that BH–BH binaries are quickly ejected from star clusters due to strong few-body interactions. This seems to confirm the model of O'Leary et al. (2006) but the simulations are too small for any strong conclusions to be drawn. It seems that star clusters can significantly enhance the rate of BH–BH mergers in the Universe however by exactly how much depends strongly on the dynamical assumptions made.

All of these simulations resolve the few-body interactions but either use very simplified models for the global cluster dynamics or have values of N too small to represent globular clusters (GCs). In this paper we use a Monte Carlo code to self-consistently model the dynamics of GCs over a range of metallicities, binary fractions and initial concentrations. We hope to constrain which dynamical assumptions are most likely to produce accurate results for GW event rate predictions. We will focus only on the compact binaries that can be found within the cluster during its evolution, leaving a detailed discussion of the population of escapers to a future paper. In Section 2 we briefly describe the Monte Carlo code and some of its features and limitations. In Section 3 we describe our initial models. In Section 4 we present the results of our simulations. In Section 5 we present predictions for LISA detections. We discuss our results in Section 6 and conclude in Section 7.

2 NUMERICAL METHODS

Monte Carlo star cluster simulations use Monte Carlo integration of the theory of two-body relaxation in order to approximate the evolution of GCs. Assuming a spherically symmetric potential, the orbit of each centre of mass (single star or binary) in the cluster at any instant can be defined by its energy, E, and angular momentum vector, $\boldsymbol{J}$. Changes in E and $\boldsymbol{J}$ due to the surrounding stars can then be calculated by an appropriate choice of random scattering events from the theory of two-body relaxation. In this way the dynamical evolution of the star cluster can be simulated self-consistently. A position for each star can be defined using a time-weighted average over the orbit defined by E and $\boldsymbol{J}$ and then the probability of encounters between stars can be calculated. Unlike other approximate methods for calculating star cluster evolution, each centre of mass is explicitly included in the simulation. Therefore it is relatively straightforward to incorporate special prescriptions for individual astrophysical events such as few-body interactions (which are not covered by the Monte Carlo approximation) and stellar evolution.

2.1 The Monte Carlo code

We use a Hénon-type code (Hénon 1971) incorporating the improvements of Stodółkiewicz (1982) and Stodółkiewicz (1986) for both global and binary dynamics as described by Giersz (1998). The code includes prescriptions for three-body binary formation and for binary–single and binary–binary encounters. The probability for three-body binary formation interactions are calculated between all adjacent stars at each time-step according to equations (7) and (8) in Giersz (2001). New energies, velocities and orbital parameters are calculated according to Giersz (1998). Binary–single and binary–binary interaction probabilities are calculated in a similar way to Giersz & Spurzem (2003). The outcome of the binary–binary interactions follow the prescriptions of Stodółkiewicz (1986) which are in turn based on the numerical experiments of Mikkola (1984). Exchange interactions, where one binary member can be exchanged for a field star or the member of another binary, are allowed during binary–single and binary–binary interactions. The most common exchange outcome is a light star being exchanged for a massive star. The probability of an exchange interaction for each star is given by equation (17) of Heggie, Hut & McMillan (1996). Tidal truncation is treated in a simplified way using the approach of Baumgardt (2001) (Giersz 2001; Giersz, Heggie & Hurley 2008).

Single and binary stellar evolution are simulated using the single stellar evolution (SSE) and binary stellar evolution (BSE) recipes of Hurley, Pols & Tout (2000) and Hurley, Tout & Pols (2002)

(Giersz et al. 2008). These recipes include a full treatment of binary and stellar evolution from the zero-age main-sequence (MS) to the degenerate remnant for a variety of stellar masses and metallicities. Of particular interest to our work are the natal velocity kicks applied to NSs and BHs due to asymmetric supernova explosions (Lyne & Lorimer 1994). Velocity kicks are applied to all NSs and BHs at birth and are drawn from a Maxwellian velocity distribution with a dispersion of $\sim$190 km s^{-1} based on Hansen & Phinney (1997)'s proper motion samples of NSs. The kick velocity of the BHs is then reduced in proportion to the mass of accreted material as described in Belczynski, Kalogera & Bulik (2002). The survivability of the binary is calculated as described in Belczynski et al. (2006). A simplified GW inspiral time-scale in the weak field limit (e.g. Peters 1964) is also included.

The code has been compared to direct N-body simulations and produces excellent agreement between global dynamical properties for both single (Giersz 1998) and multimass cases (Giersz 2001, 2006). Giersz et al. (2008) have shown the code compares very well with direct N-body simulations when stellar evolution is included. The code is also able to re-produce several observed physical parameters, such as the surface brightness profiles and luminosity functions, of the observed star clusters M67 (Giersz et al. 2008), M4 (Heggie & Giersz 2008) and NGC 6397 (Giersz & Heggie 2009).

An attractive feature of Monte Carlo simulations is that the computation scales with $\mathcal{O}(N^1)$–$\mathcal{O}(N^2)$ rather than the $\mathcal{O}(N^3)$ of direct N-body codes. Furthermore, including binaries does not greatly decrease the performance. This means that a simulation of $N \approx 5 \times 10^5$–10^6 bodies with 50 per cent binaries can be carried out on a single fast processor in the order of hours to days rather than the weeks to months required for direct N-body simulations. At the same time, unlike other approximate methods of calculating star cluster evolution, the Monte Carlo simulation manages to provide the same star-by-star information produced by direct N-body codes. Thus the Monte Carlo code can be used for large parameter studies in a short space of time where the details of individual stellar events, such as inspirals and mergers, are of interest.

2.2 Limitations

The approximations used in the Monte Carlo code introduce limitations that may affect our results. In particular the BHs may be sufficiently massive compared to the rest of the system that become 'Spitzer unstable' (Spitzer 1987) and form a decoupled small N subsystem in the cluster core. This subsystem interacts only with itself and in such a situation if N becomes small enough the distinction between large and small angle scattering breaks down. The Monte Carlo approximation relies on the fact that these scales may be separated (the cluster can be divided into a near and far zone) and may become unreliable for small Spitzer unstable subsystems. Giersz (2001, 2006) has shown that the Monte Carlo code accurately re-produces binary burning in the cluster core, indicating that the code can resolve the statistical properties of strong interactions in dense regions well. Furthermore, Heggie & Giersz (2009) have compared direct N-body and Monte Carlo simulations for the case of the cluster NGC 6397 and have shown good agreement both for the escape rate (driven by ejections from the core) and binary energy generation. Thus despite its limitations, the Monte Carlo code still seems to be able to produce statistically reliable results for strongly interacting regions. We will also be able to compare our results to those of O'Leary et al. (2006), who make the explicit assumption of a Spitzer unstable BH population, in order to constrain this effect. Furthermore, if there are a large number of BHs in the cluster any Spitzer unstable subsystem that they may form will be large enough that the Monte Carlo approximation remains valid.

Another issue is our treatment of strong few-body interactions. Our code currently uses analytic cross-sections calculated in Heggie (1975), Mikkola (1984), Stodółkiewicz (1986) and Heggie et al. (1996) for the initialization and outcome of binary–single and binary–binary interactions and three-body binary formation. For unequal mass cases these cross-sections are not certain and only allow a limited range of outcomes. Another problem is that lacking explicit orbital integration, mergers are only possible if the stellar radii overlap at the conclusion of an interaction, ignoring the effect of close approaches during the interaction. Thus we will probably underestimate the number of compact binary mergers in our simulation. We note that ideally we would include a few-body integrator in the Monte Carlo code as has been done by Fregeau & Rasio (2007) or in the context of a gas–Monte Carlo hybrid code by Giersz & Spurzem (2003). Such work is planned for the future but will inevitably slow down the code considerably, making large parameter studies more difficult.

3 CLUSTER MODELS

We have preformed simulations of star clusters with 16 different sets of initial conditions. Each simulation has 5.0×10^5 centres of mass (single stars or binaries). All simulations use a Kroupa initial mass function (IMF; Kroupa, Tout & Gilmore 1993), a broken power law with a low-mass slope of $\alpha_{\rm l} = 1.3$, a high-mass slope of $\alpha_{\rm h} = 2.3$ and a break mass of $M_{\rm break} = 0.5\,{\rm M}_\odot$. We follow Sadowski et al. (2008) and choose masses between 0.1 and 150 $\rm M_\odot$. All simulations are initialized as Plummer models with a tidal cut-off at $r_{\rm tc} = 150$ pc. According to the classical formula of Spitzer (1987):

$$r_{\rm tc}^3 = \frac{M_{\rm C}}{2M_{\rm G}} R_{\rm G}^3, \tag{1}$$

where $M_{\rm C}$ is the mass of the cluster, $M_{\rm G}$ is the mass of the galaxy and $R_{\rm G}$ is the galactocentric radius. For a galactic mass of $\approx 6 \times 10^{10}\,{\rm M}_\odot$ and our cluster masses (Table 1) this yields $R_{\rm G} \sim$ 9–10 kpc, a

Table 1. The initial conditions for our simulations. Column 1 gives the model, column 2 the initial binary fraction, column 3 the metallicity, column 4 the initial ratio of tidal to half-mass radius, column 5 the initial mass and column 6 the initial half-mass relaxation time. Both columns 5 and 6 are averaged all 10 independent realizations.

	Initial conditions				
Simulation	$f_{\rm b}$	Z	$r_{\rm t}/r_{\rm h}$	M ($\rm M_\odot$)	$t_{\rm rh}$ (Myr)
10sol21	0.1	0.02	21	3.61×10^5	3.54×10^3
10sol37	0.1	0.02	37	3.63×10^5	1.51×10^3
10sol75	0.1	0.02	75	3.62×10^5	5.25×10^2
10sol180	0.1	0.02	180	3.63×10^5	1.41×10^2
50sol21	0.5	0.02	21	5.08×10^5	2.99×10^3
50sol37	0.5	0.02	37	5.08×10^5	1.28×10^3
50sol75	0.5	0.02	75	5.06×10^5	4.44×10^2
50sol180	0.5	0.02	180	5.09×10^5	1.19×10^2
10low21	0.1	0.001	21	3.60×10^5	3.55×10^3
10low37	0.1	0.001	37	3.62×10^5	1.51×10^3
10low75	0.1	0.001	75	3.62×10^5	5.25×10^2
10low180	0.1	0.001	180	3.63×10^5	1.41×10^2
50low21	0.5	0.001	21	5.08×10^5	2.99×10^3
50low37	0.5	0.001	37	5.07×10^5	1.28×10^3
50low75	0.5	0.001	75	5.07×10^5	4.44×10^2
50low180	0.5	0.001	180	5.07×10^5	1.19×10^2

distance just beyond the solar orbit. Since we do not include disc shocking in our models, these represent halo clusters. We choose relatively isolated initial conditions to ensure that the effects we observe are due to internal cluster dynamics and yet can still investigate escapers. The tidal cut-off is not held constant during the evolution of the cluster but is recalculated at each time-step according to the current cluster mass. There is an N-dependent parameter, α, that describes a modification of the tidal radius necessary to produce an agreement in escape rate between direct N-body models and the Monte Carlo code (Baumgardt 2001; Giersz et al. 2008). It is set to 1.31 in our simulations which is the value chosen for the M4 models described in Heggie & Giersz (2008). These models have a similar number of particles to the simulations described in this paper and agree well with observations.

We use two different metallicities for our simulations: $Z_{\rm h} = 0.02$ and $Z_{\rm l} = 0.001$. $Z_{\rm h}$ corresponds roughly to solar metallicity while $Z_{\rm l}$ corresponds both to the low-metallicity peak of the Galactic GC distribution and, for comparison purposes, to the metallicity chosen by Sadowski et al. (2008). These two metallicities also fall within the high- and low-mass peaks in the bimodal metallicity distribution found for brightest cluster galaxies by Harris et al. (2006). For the purpose of our study the primary difference between these metallicities is the treatment of stellar mass loss in the BSE code. The mass of single BHs is calculated according to Belczynski et al. (2002). In these prescriptions mass loss is suppressed at low metallicity due to less efficient line driving of stellar winds and this allows the formation of significantly more massive BHs. These high-mass BHs mass segregate more swiftly than their low-mass counterparts and will be stronger GW sources. The initial distribution of BH masses these prescriptions yield is studied in detail in Belczynski et al. (2006).

We also use two different binary fractions: $f_{\rm b} = 0.1$ and $f_{\rm b} = 0.5$. Thus, while they have the same total number of centres of mass, simulations with $f_{\rm b} = 0.1$ have 5.5×10^5 stars whereas simulations with $f_{\rm b} = 0.5$ have 7.5×10^5 stars. The simulations with $f_{\rm b} = 0.5$ will be more massive and produce a larger total number of BHs simply because there are more stars present. $f_{\rm b} = 0.5$ will also produce more binary–single and binary–binary interactions due to the larger number of primordial binaries. This in turn will increase the probability of exchange interactions and increase the number of BHs introduced into binaries. The initial binary parameters are produced using the eigenvalue evolution and feeding algorithms of Kroupa (1995). These prescriptions use a thermal distribution of birth eccentricities ($f(e_{\rm b}) = 2e_{\rm b}$), birth mass ratios ($q_{\rm b}$) drawn at random from the Kroupa et al. (1993) IMF and a birth period distribution of

$$f(P_{\rm b}) = 2.5\frac{\log P_{\rm b} - 1}{45 + (\log P_{\rm b} - 1)^2} \tag{2}$$

with the limits $\log P_{\rm b,min} = 1$ and $\log P_{\rm b,max} = 8.43$. These birth values are then modified according to the eigenvalue and feeding algorithm to simulate the effect of pre-MS evolution. Initial eccentricities are calculated as

$$\ln e_{\rm in} = -\rho + \ln e_{\rm b}, \tag{3}$$

where

$$\rho = \int_0^{\Delta t} {\rm d}t\ \rho' = \left(\frac{\lambda {\rm R}_\odot}{R_{\rm peri}}\right)^{\chi}, \tag{4}$$

where ρ'^{-1} is the circularization time-scale, $\Delta t \approx 10^5$ yr is the pre-MS evolution time-scale, $R_{\rm peri}$ is the pericentre distance of the binary and $\lambda = 28$ and $\chi = 0.75$ are empirically determined constants. The initial mass ratio is given by

$$q_{\rm in} = q_{\rm b} + (1 - q_{\rm b})\rho^\star, \tag{5}$$

where

$$\rho^\star = \begin{cases} \rho & \rho \le 1, \\ 1 & \rho > 1, \end{cases} \tag{6}$$

where the mass of the secondary is modified according to $m_{2,\rm in} = q_{\rm in}\ m_{2,\rm b}$ and the mass of the primary is unchanged $m_{1,\rm in} = m_{1,\rm b}$. Finally the period is given by

$$P_{\rm in} = P_{\rm b}\left(\frac{m_{\rm t,b}}{m_{\rm t,in}}\right)^{1/2}\left(\frac{1 - e_{\rm b}}{1 - e_{\rm in}}\right)^{3/2}, \tag{7}$$

where $m_{\rm t,b}$ and $m_{\rm t,in}$ are the total masses before and after the application of equation (5). The main effect of the eigenvalue and feeding evolution is to depopulate the short-period, high-eccentricity area of the period–eccentricity diagram as observed in Galactic binaries. The initial period distribution and the effect of the eigenvalue feeding can be seen in figs 1 and 2 of Kroupa (1995). The effect of a dense stellar environment on generic binary populations has been investigated in several sources such as Heggie (1975) and Portegies Zwart et al. (2004). The Kroupa (1995) prescriptions also provide a good match to the binary parameters observed in the Galactic field.

We have performed simulations with four initial concentrations that we control using the ratio of the initial tidal radius to the initial half-mass ($r_{\rm h}$). We use initial ratios of $r_{\rm t}/r_{\rm h} = 21$, 37, 75 and 180, corresponding to initial number densities within $r_{\rm h}$ of $\sim 10^2$, 10^3, 10^4 and 10^5, respectively. The initial concentration primarily affects the half-mass relaxation time ($t_{\rm rh}$), defined by Spitzer (1987) as

$$t_{\rm rh} = 0.138\frac{N^{1/2} r_{\rm h}^{3/2}}{\langle m\rangle^{1/2} G^{1/2} \ln\gamma N}, \tag{8}$$

where N is the total number of centres of mass in the system, $\langle m\rangle$ is the average mass, $\ln\gamma$ is the Coulomb logarithm and γ is an empirically fitted parameter. The value of γ is different for single and multimass systems and has been debated in the literature. For equal-mass systems $\gamma = 0.11$ seems to be favoured (Giersz & Heggie 1994) whereas for multimass systems $\gamma = 0.02$ gives better results (Giersz et al. 2008). We choose $\gamma = 0.02$ for our simulations but have rerun one set, 50low75, with $\gamma = 0.11$ for comparison purposes. The results will be discussed in Section 4. The simulations all have a fixed initial tidal cut-off and thus the more concentrated simulation have smaller values of $r_{\rm h}$. Thus, according to equation (8), they will also have shorter values of $t_{\rm rh}$ and will evolve, dynamically speaking, more quickly than their less concentrated counterparts. Whatever effect dynamics have on the production of BH–BH binaries should be accelerated in these systems.

Since star cluster dynamics are stochastic and chaotic, large fluctuations can occur between different realizations of the same simulation (e.g. Giersz et al. 2008; Heggie & Giersz 2008; Giersz & Heggie 2009). For this reason we perform 10 independent realizations of each combination of initial conditions differing only by the initial random seed. Thus we have a total of 160 simulations to analyse. To ensure that 10 simulations are enough for convergence we have extended two of the simulations, 10sol75 and 50low75, to 50 simulations and will compare the number of BH–BH binaries produced in Section 4. Table 1 gives the initial parameters of our 16 different sets of simulations, averaged over all 10 realizations. Each simulation is run on a single processor at the HLRS supercomputer in Stuttgart. The shortest simulations (10sol21) take $\sim$4 h to complete and the longest (50low180) take $\sim$12–16 h.

4 RESULTS

We find no more than one or two NS–NS or NS–BH binaries over the course of an entire Hubble time in any of our simulations and no NS–NS or NS–BH mergers. For this reason we only present results for the BH–BH binary population. The lack of NS–NS and NS–BH binaries is due to the fact that few primordial binaries survive to a phase where they would contain an NS or BH since most merge during mass transfer and those that do are disrupted at the second supernova. As we will show, our BH–BH binaries are not primordial but rather form dynamically, a process that occurs most efficiently for massive objects. Since the BHs are, for the most part, significantly more massive than the NSs in our simulations, they will be preferentially exchanged into binaries until they are depleted. None of our simulations is completely depleted of BHs after one Hubble time and thus the NSs have little opportunity to take part in dynamical compact binary formation. We do not analyse the (large) WD–WD population but save these results for a future paper.

In Table 2 we show the total number of BHs formed both in isolation and in binaries in each simulation averaged over all 10 independent realizations. For each simulation the rms scatter across the independent realizations is small and is merely a result of random sampling of the IMF. The number of BHs formed is not a function of concentration in any range of Z or f_b. This is not surprising since BHs are produced primarily by individual stellar evolutionary processes. It is possible that extra BHs could be produced by stellar collisions in which two stars below the critical mass to produce a BH merge to form a single star above the critical mass. Collisions would be expected to be more frequent in dense clusters but this effect does not seem to produce a significant enhancement in the number of BHs in our simulations. The number of BHs formed depends on f_b because a higher binary fraction corresponds to a larger number of stars, and on Z because mass loss is less efficient at low metallicity and stars with a lower zero-age MS mass can become BHs. Proportionately more BHs are formed in binaries at $f_b = 0.5$ than at $f_b = 0.1$ but this is simply a consequence of the larger fraction of stars found in binaries at high f_b. It is apparent from column 5 of Table 2 that very few of the binaries that form a single BH survive its formation; most either merge or are disrupted at the supernovae. Furthermore, very few binaries where both members are BHs form directly from primordial binaries and of those *all* are disrupted during the formation of the second BH. Therefore all BH–BH binaries produced by our simulations must be formed by dynamical means. There is no difference in either the mean number or the rms scatter in BHs produced in either of the simulations for which we have performed an extended number of realizations. We therefore conclude that 10 simulations are sufficient to produce accurate statistics on the BH population produced by stellar evolution.

In Table 3 we present the cumulative number of BH–BH binaries that have existed in each simulation up to the dynamical time shown and after one Hubble time ($T_H = 14$ Gyr). The ages 3 t_{rh}, 9 t_{rh} and 25 t_{rh} correspond, respectively, to the dynamical age of the clusters with $r_t/r_h = 21$, 37 and 75 at $\approx 1T_H$. The simulations with $r_t/r_h = 180$ have a dynamical age of $\sim$115–120t_{rh} at $1T_H$. A new BH–BH binary is counted every time a binary where both members are BHs forms. Both a binary with one BH and one MS star where the MS star is exchanged for a BH and a binary where both members are BHs and one of the BHs is exchanged for a new BH are counted as new BH–BH binaries. The rms scatter in the number of BH–BH binaries produced by different realizations of the same simulation in Table 3 is significantly larger than for Table 2. This is because, unlike stellar evolution, dynamical binary formation is a stochastic process,

Table 2. Number of BHs formed in each model by stellar evolutionary processes. N_{sBH} is the total number of BHs formed in the cluster, N_{bBH} the total number of BHs formed in binaries. N_{BHBH} is the total number of BH–BH binaries formed by stellar evolutionary processes and N_{surv} is the number of binaries that form a single BH and survive the formation process. All primordial BH–BH binaries are disrupted during the second supernovae. Each quantity is averaged over all 10 independent realizations and includes the rms scatter.

	Individual BH statistics			
Simulation	$N_{sBH} \pm \sigma$	$N_{bBH} \pm \sigma$	$N_{BHBH} \pm \sigma$	$N_{surv} \pm \sigma$
10sol21	1103 ± 18	197 ± 8	2 ± 1	0 ± 0
10sol37	1119 ± 44	206 ± 17	3 ± 2	0 ± 0
10sol75	1104 ± 31	200 ± 12	2 ± 1	0 ± 0
10sol180	1129 ± 22	190 ± 18	3 ± 1	0 ± 0
50sol21	1495 ± 43	976 ± 35	13 ± 5	0 ± 1
50sol37	1515 ± 32	989 ± 28	12 ± 4	0 ± 0
50sol75	1498 ± 28	978 ± 29	9 ± 2	0 ± 1
50sol180	1555 ± 42	956 ± 36	9 ± 3	0 ± 0
10low21	1248 ± 34	217 ± 19	2 ± 2	0 ± 1
10low37	1262 ± 30	228 ± 18	4 ± 2	0 ± 1
10low75	1265 ± 30	229 ± 14	5 ± 4	0 ± 1
10low180	1296 ± 37	227 ± 18	3 ± 2	0 ± 1
50low21	1719 ± 46	1090 ± 25	8 ± 2	3 ± 2
50low37	1728 ± 47	1124 ± 45	17 ± 4	3 ± 2
50low75	1731 ± 37	1125 ± 39	16 ± 3	2 ± 1
50low180	1769 ± 31	1077 ± 33	9 ± 3	4 ± 3
	With 50 realizations			
10sol75	1099 ± 29	201 ± 14	2 ± 1	0 ± 0
50low75	1746 ± 38	1132 ± 29	18 ± 4	3 ± 2

Table 3. The cumulative number of BH–BH binaries after 3, 9 and 25t_{rh}, and also after $1T_H$. Each column is averaged over all 10 independent realizations and includes the rms scatter. A dash in a column indicates that the cluster did not reach that number of half-mass relaxation times within $1T_H$s.

	BH–BH binaries after xt_{rh}			
Simulation	$t = 3\ t_{rh}$	$t = 9\ t_{rh}$	$t = 25\ t_{rh}$	$t = 14$ Gyr
10sol21	1 ± 1	–	–	1 ± 1
10sol37	1 ± 1	14 ± 11	–	14 ± 11
10sol75	0 ± 1	8 ± 6	49 ± 19	52 ± 19
10sol180	0 ± 0	12 ± 6	54 ± 21	123 ± 27
50sol21	1 ± 1	–	–	3 ± 2
50sol37	3 ± 2	36 ± 10	–	50 ± 11
50sol75	1 ± 1	26 ± 8	115 ± 24	147 ± 28
50sol180	0 ± 1	11 ± 5	111 ± 23	354 ± 33
10low21	22 ± 10	–	–	27 ± 10
10low37	23 ± 4	44 ± 6	–	44 ± 6
10low75	18 ± 10	32 ± 13	54 ± 6	54 ± 16
10low180	26 ± 8	51 ± 8	79 ± 20	112 ± 24
50low21	104 ± 16	–	–	127 ± 16
50low37	93 ± 22	175 ± 29	–	184 ± 29
50low75	64 ± 10	155 ± 22	173 ± 22	202 ± 38
50low180	103 ± 19	205 ± 35	294 ± 50	453 ± 109
	With 50 realizations			
10sol75	0 ± 1	7 ± 4	38 ± 20	41 ± 21
50low75	78 ± 15	175 ± 29	232 ± 43	245 ± 48

strongly dependent on chance encounters that are a function of the detailed dynamics of the specific system, and, since all BH–BH binaries are formed dynamically, large system-to-system variations are expected. Again we find that for the two simulations where we performed additional independent realizations, the additional realizations provide no difference in the size of the rms scatter and the average number of BH–BH binaries at each relaxation time is the same to within the rms scatter. Therefore we conclude that 10 realizations are also enough to constrain the statistics of the dynamical processes and we retain this number for the rest of our analysis.

There are some clear trends in Table 3. After $1T_{\rm H}$ the number of BH–BH binaries increases with $f_{\rm b}$ and initial concentration and decreases with Z. The reasons for the $f_{\rm b}$ correlation are clear: a larger number of both BHs and hard binaries for the BHs to be exchanged into. The correlation with initial concentration is related to the relative dynamical ages of the clusters after $1T_{\rm H}$. For the same $f_{\rm b}$ and Z the simulations have roughly the same number of BH–BHs when compared at the same dynamical age. By $1T_{\rm H}$, however, clusters with a higher initial concentration are dynamically older and have had more opportunity to produce BH–BH binaries than their dynamically younger counterparts. The correlation with Z is due to the higher mass BHs present at low metallicity. Since the mass-segregation time-scale, $t_{\rm eq}$, (for a two-component system) scales as (Spitzer 1987)

$$t_{\rm eq} \propto t_{\rm rh} \frac{m_1}{m_2}, \tag{9}$$

where $m_2 > m_1$ (Watters, Joshi & Rasio 2000; Khalisi, Amaro-Seoane & Spurzem 2007), we expect more massive BHs to mass segregate more rapidly than less massive ones. This accelerates the process of BH–BH binary formation since the core is the densest region and is where most dynamical binary formation will take place. The more massive BHs are also more likely to be retained by the cluster since they will need larger kicks upon formation in order to reach escape velocity.

We have also considered a different value of γ and we present these results in Fig. 1. According to equation (8), the effect of increasing γ is to reduce $t_{\rm rh}$ by the logarithm of the same factor. Thus the simulations with $\gamma = 0.11$ are slightly more dynamically evolved after $1T_{\rm H}$ that the simulations with $\gamma = 0.02$. Consequently these simulations produce a few more BH–BH binaries. The increase, however, is small and the average values for both sets of simulations fall within each others rms scatter. We conclude that any reasonable changes in γ will not affect our results in any important way.

Fig. 2 shows the number of BH–BH binaries in each simulation per Gyr. The trends noted in Table 3 are apparent, particularly those associated with the initial concentration. Simulations with higher initial concentration have a peak number of BH–BH binaries per unit time much earlier than those with lower concentration. Those with lower concentration sustain more constant but lower BH–BH populations over longer spans of physical time. It is also clear that the more metal-poor simulations evolve more quickly and produce BH–BH binaries earlier than their metal-rich counterparts. This again is a consequence of faster mass segregation. Finally, $f_{\rm b}$ does not affect the time of peak BH–BH binary number but simulations with $f_{\rm b} = 0.5$ are able to sustain production of BH–BH binaries longer because the supply of BHs and hard binaries to exchange them into is larger in these clusters.

In Fig. 3 we investigate the spatial distribution of the BHs and BH–BH binaries in each simulation by comparing the half-mass radius of each species to the half-mass radius of the entire cluster. In all cases single BHs are centrally concentrated compared to the rest of the stars. This is simply a consequence of mass segregation. The varying mass segregation time-scales can be seen in the length of time taken for the half-mass radii of the BH populations to contract to an equilibrium state caused by binary burning. The half-mass radii of the BH–BH populations must be interpreted more carefully. Since BH–BH binaries are formed dynamically in cluster cores, the BH–BH binary populations are initially very centrally concentrated. As the population evolves, however, the BH–BH binaries interact strongly and can eject each other from the core region. As is clear from Fig. 2 there are often very few BH–BH binaries in the cluster, even over a span of 1 Gyr, and thus the half-mass radius of the BH–BH population in Fig. 3 is often based on quite a small number of objects. Thus the location of a single massive BH–BH binary can dominate the determination of the half-mass radius of the BH–BH binary population. Overall it is clear that BH–BH binaries form in the cluster core and tend to be centrally concentrated but they are not necessarily more concentrated than the single BH population. Individual BH–BH binaries may also exit in the outskirts of the cluster for a time if they are ejected from the core by dynamical interactions and before they have a chance to sink back to the centre due to dynamical friction.

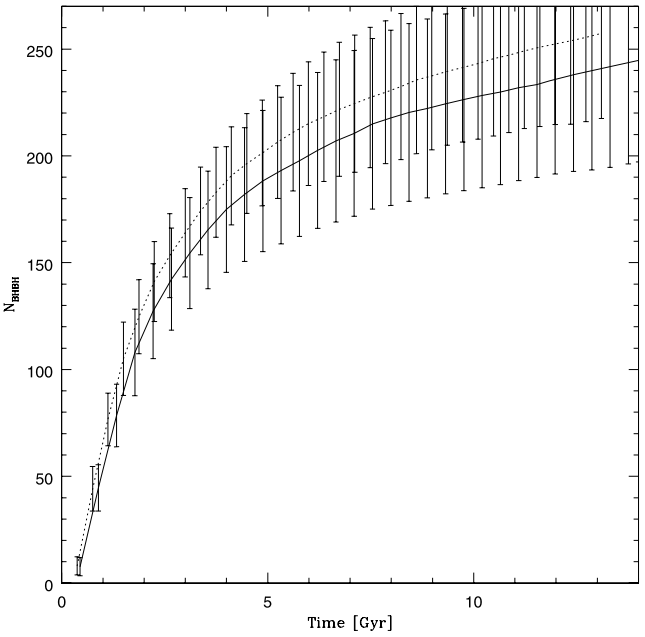

Figure 1. Run 50low75 for two values of γ: $\gamma = 0.02$ (solid) and $\gamma = 0.11$ (dotted). $\gamma = 0.11$ has a slightly shorter relaxation time and produces slightly more BH–BH binaries after a Hubble time but both agree to within the rms error.

It is also worth noting that the BH–BH binaries will not be strongly affected by interactions with anything other than BHs. The comparative masses mean that other stars do not have sufficient energy to disrupt or scatter the BH–BH binaries. Conversely the BH–BH binaries will have a very strong effect on the other stars they encounter and will be the major energy source in the cluster core. Thus BH–BH binaries are only affected by each other but have a major influence on core dynamics.

The cumulative chirp mass ($M_{\rm chirp} = (M_1\,M_2)^{3/5}/(M_1 + M_2)^{1/5}$) distribution for all BH–BH binaries that have existed in the simulations up to $1T_{\rm H}$ are given in Fig. 4. We choose to display $M_{\rm chirp}$

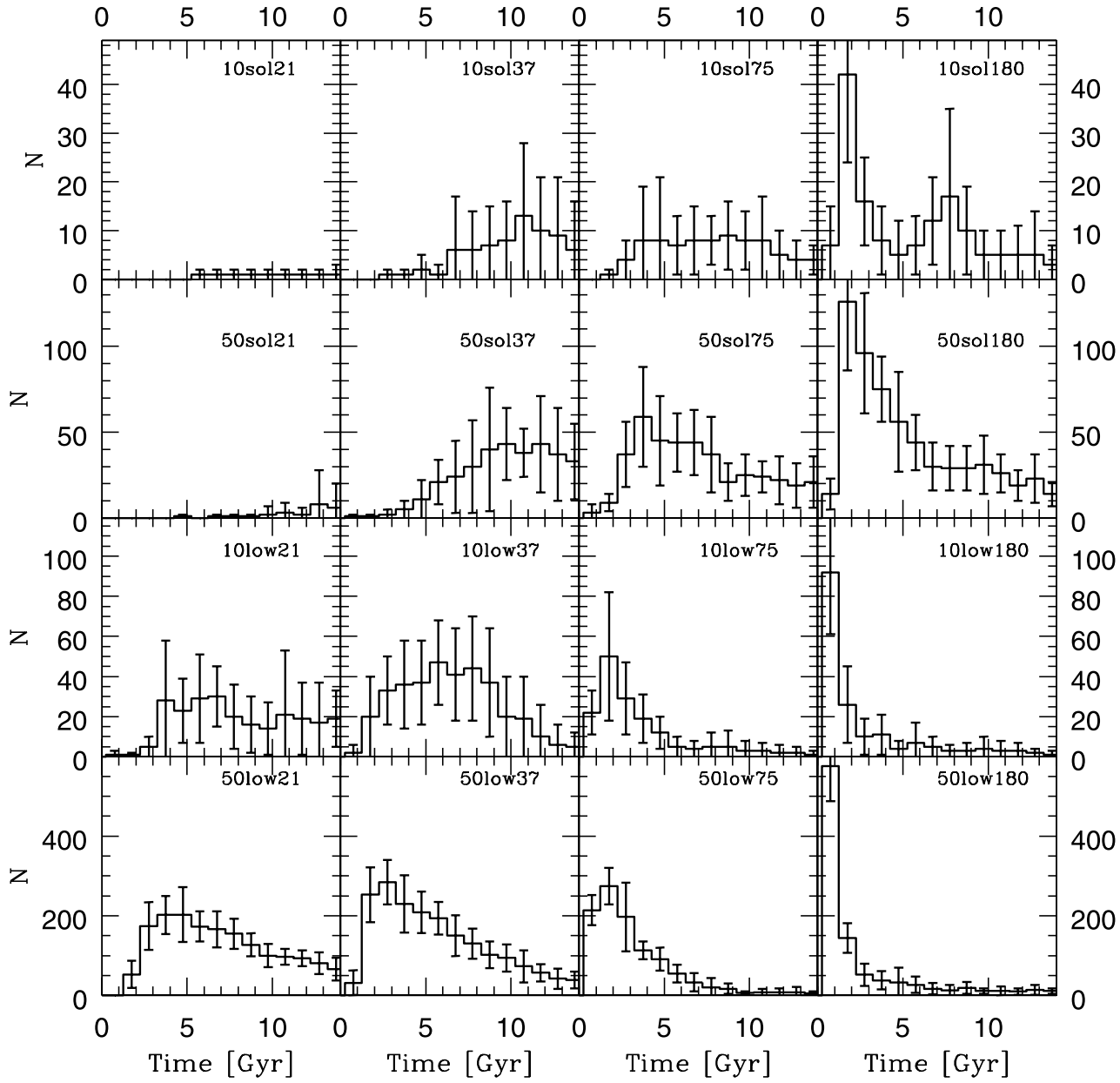

Figure 2. The number of BH–BH binaries per Gyr for each of the 16 sets of initial conditions. Each time bin is averaged over all 10 independent realizations and the error bars represent the rms scatter.

rather than the total mass because the amplitude of gravitational radiation, h_0, scales as

$$h_0 \propto \frac{G^{5/3}\omega^{2/3}M_{\rm chirp}^{5/3}}{rc^4} \tag{10}$$

(Pierro et al. 2001). Thus it is $M_{\rm chirp}$ and not the total mass of the binary that is significant for GW detection. For the high-metallicity simulations the distribution of chirp masses is narrow with a peak around 8–10 $M_\odot$. The distribution is not affected by any of the other initial conditions. The low-metallicity distribution is broader and fairly flat between 10 and 20 $M_\odot$. This is a direct consequence of the more massive BHs generated at lower metallicity. Here the distribution is weakly affected by the initial concentration with $M_{\rm chirp}$ peaking at lower masses for the more concentrated simulations. This is a result of the relative dynamical ages of the simulations as we demonstrate in Fig. 5, the distribution of $M_{\rm chirp}$ after 9 $t_{\rm rh}$. At the same dynamical age the mass distribution is unaffected by the concentration. Recalling equation (9), the more massive BHs will mass segregate before the less massive BHs and thus interact and be disrupted or ejected earlier. Only then will low-mass BHs participate in BH–BH binary formation. Since the more concentrated clusters are dynamically older, they have had more time to experience this effect, deplete their high-mass BHs and have a lower mass BH–BH binary population. The high-metallicity clusters do not have a broad enough distribution in mass for this effect to be important. Perhaps the most interesting result is that after $1T_{\rm H}$ the $M_{\rm chirp}$ distributions are systematically different between clusters with different metallicities and concentrations. Building an $M_{\rm chirp}$ distribution from GW observations can yield information on the physical and dynamical state of GCs.

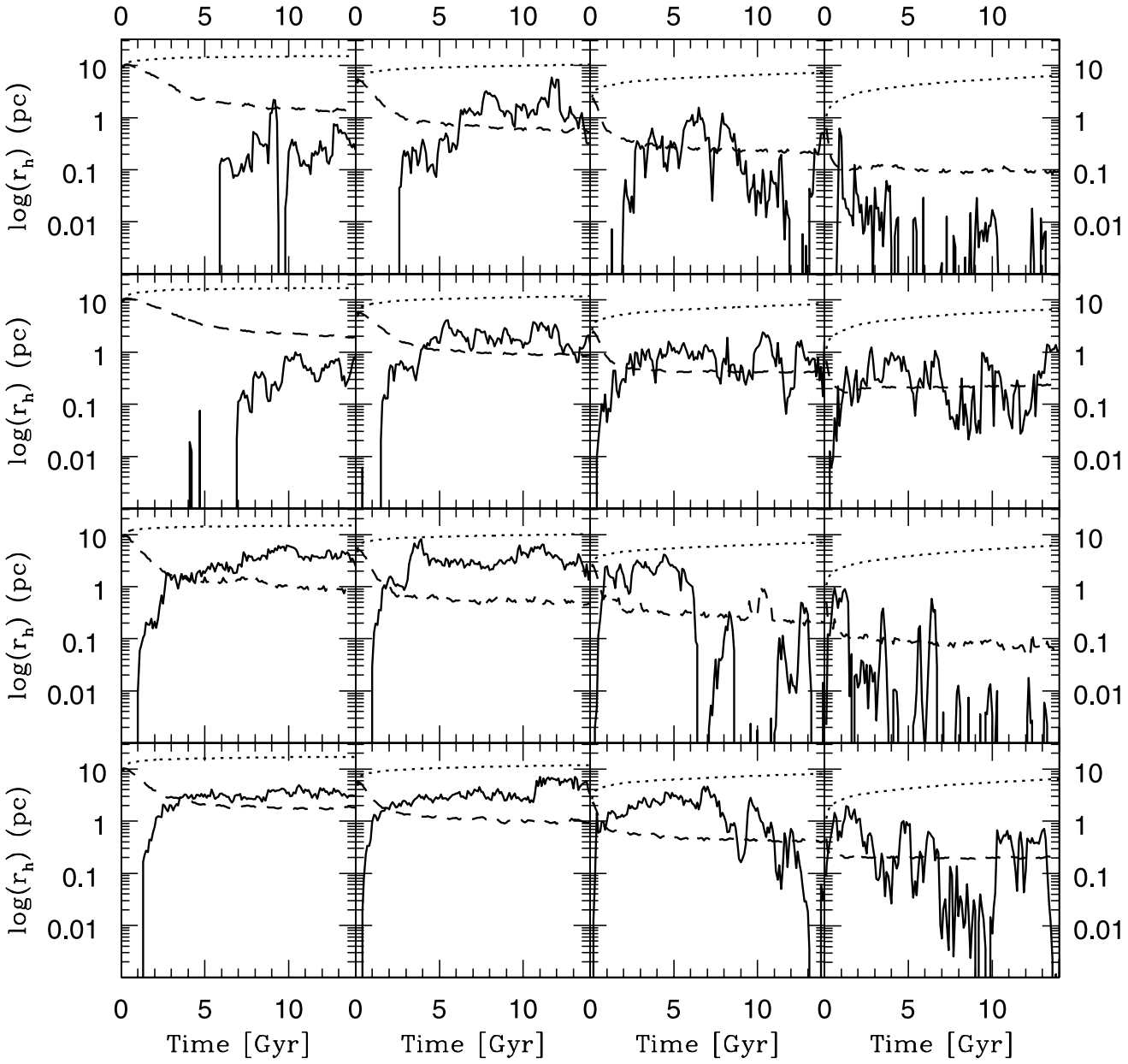

Figure 3. The half-mass radii for the BH system. Top to bottom: $Z = 0.02$ and $f_b = 0.1$, $Z = 0.02$ and $f_b = 0.5$, $Z = 0.001$ and $f_b = 0.1$ and $Z = 0.001$ and $f_b = 0.5$. Left to right: $r_t/r_h = 21,\ 37,\ 75$ and 180. Shown are cluster r_h (dotted), r_h of all BHs (dashed) and r_h of all BH–BH binaries (solid). The radial profiles have been boxcar smoothed with a 100 Myr box and each box has been averaged across all 10 independent realizations.

The cumulative distribution of BH–BH binary binding energy (E_{bind}) up to $1T_H$ is given in Fig. 6. The energy is given in units of the thermal energy of the core of the cluster:

$$k_B T = (m_{core}/2N_{core})\sigma^2_{core}, \quad (11)$$

where m_{core} is the total core mass, N_{core} the number of stars in the core and σ_{core} the velocity dispersion in the core. The core quantities are chosen because the BH–BH binaries are formed and interact in the core, making this region the most relevant for the dynamics. All BH–BH binaries are hard. This is to be expected because soft binaries would be destroyed by the interactions necessary to introduce a BH into them. There is little variation with the cluster parameters because $k_B\ T$, the normalization factor for E_{bind}, scales with core mass and density. The only exception to this appears to be clusters with $r_t/r_h = 180$ where there are an excess of soft binaries. The combination of the larger interaction cross-section for binaries with larger semimajor axes and the larger interaction rate in the cores of very dense clusters may lead to more BHs being exchanged into softer binaries in the high-density simulations. It could also be that the soft binaries in the more concentrated simulations still have a larger binding energy in physical units than those in the less concentrated simulations and have a slightly better chance of survival.

In Fig. 7 we present the cumulative period (P) distribution of all BH–BH binaries up to $1T_H$. There is a large spread in P, ranging from days to $\sim 10^5$ yr. The period distribution does not depend strongly on the cluster parameters. The entire distribution is shifted slightly towards short periods in the more concentrated simulations. This is partly due to the slightly higher velocity dispersion in these clusters and consequently the higher value of $k_B\ T$ in physical units. Thus in concentrated clusters binaries must have higher binding

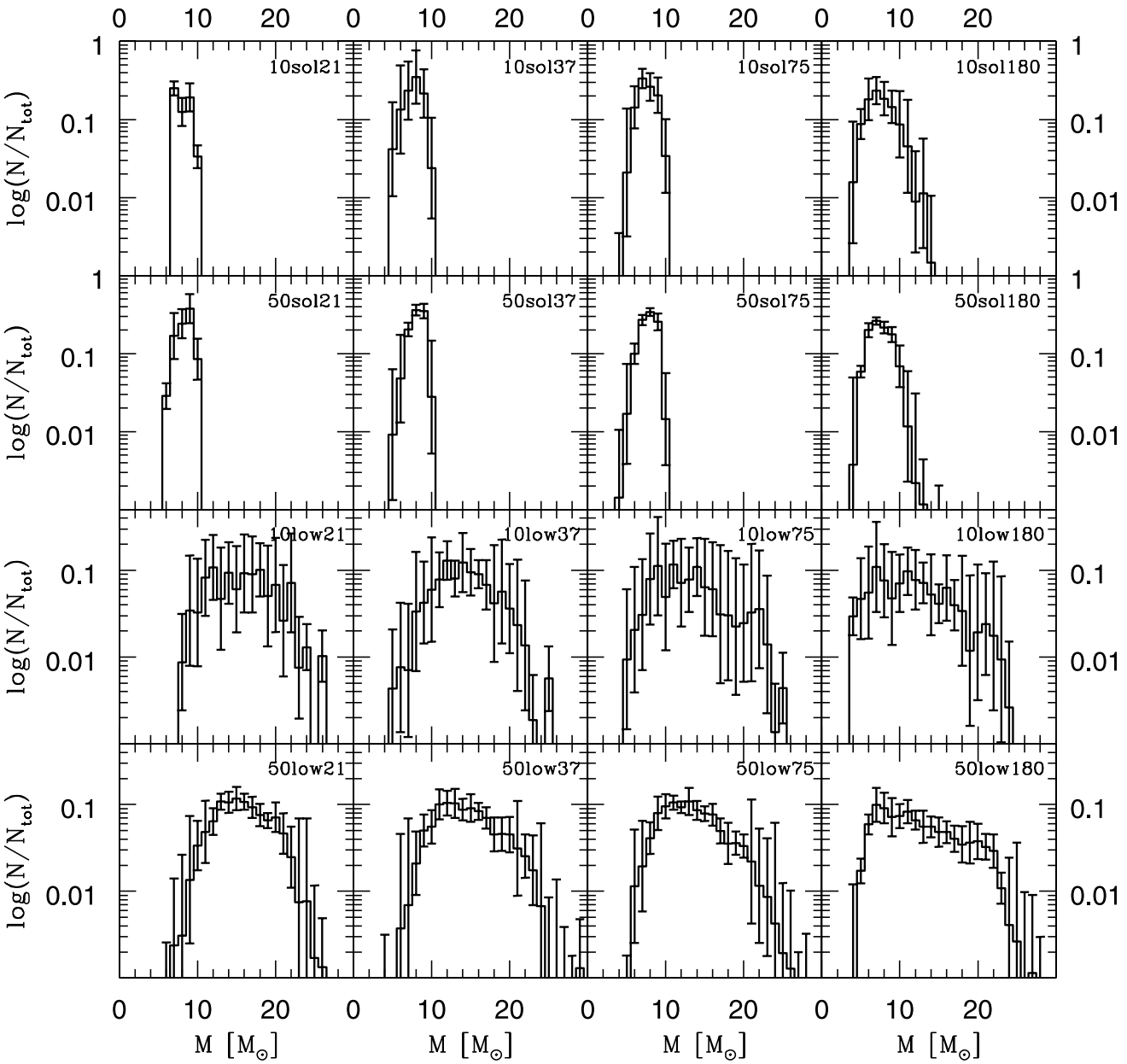

Figure 4. The cumulative chirp mass distribution of BH–BH binaries up to $1T_{\rm H}$ binned in $1\,{\rm M}_{\odot}$ bins. Each bin in each panel is averaged over all 10 independent realizations and the error bars give the rms scatter.

energies and consequently shorter periods in order to be above the hard–soft boundary (such as it is in multimass systems). It is also partly a product of the larger number of hardening interactions due to the higher interaction rate. Despite the overall shift, the clusters with $r_{\rm t}/r_{\rm h} = 180$ show a peak in at the longer end of the distribution. This simply reflects the peak at low binding energy seen in Fig. 6. Overall, however, the period distributions are similar and span approximately the same range for all models.

Although there are some binaries with periods less than a year present in most simulations, most binaries do not have sufficiently short periods to produce GW mergers within $1T_{\rm H}$. According to Peters (1964) the rate of semimajor axis decay, $\dot{a}$, for a binary emitting GWs in the orbit-averaged regime is

$$\langle \dot{a} \rangle = -\frac{64}{5} \frac{G^3 m_1 m_2 (m_1 + m_2)}{c^5 a^3 (1 - e^2)^{7/2}} \left(1 + \frac{73}{74} e^2 + \frac{37}{96} e^4\right), \quad (12)$$

where m_1 is the mass of the primary, m_2 is the mass of the secondary, e is the eccentricity and a is the semimajor axis. We can calculate an approximate inspiral time, $t_{\rm in}$, for a binary by taking

$$t_{\rm in} \approx \frac{a_{\rm in}}{\dot{a}}, \quad (13)$$

where $a_{\rm in}$ is the initial semimajor axis of a binary. For a circular binary with $m_1 = m_2 = 10\,{\rm M}_{\odot}$ and an initial period of $P_{\rm in} = 1\,{\rm d}$, $t_{\rm in} \approx 1\,{\rm Gyr}$. If $P_{\rm in} = 1\,{\rm yr}$ then $t_{\rm in} = 10^6\,{\rm Gyr}$. Thus all but the shortest period binaries in our clusters will be unable to merge within $1T_{\rm H}$. Furthermore, the minimum GW frequency for which LISA is sensitive is $\approx 10^{-5}\,{\rm Hz}$. For circular binaries all power is emitted in the $n = 2$ harmonic of ω (Peters & Mathews 1963; Belczynski et al. 2008). Thus for circular binaries to be detected by LISA they must have periods of less than a day.

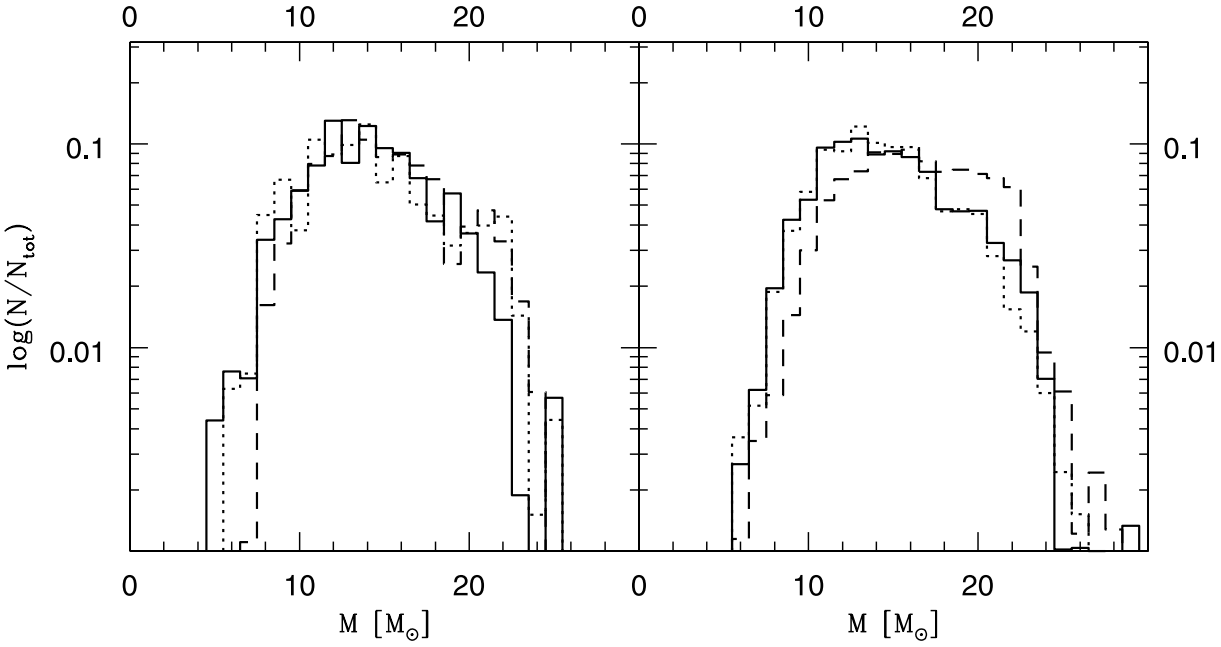

Figure 5. The cumulative chirp mass distribution of BH–BH binaries up to 9 $t_{\rm rh}$ for six simulations binned in 1 $M_\odot$ bins. Both plots are for $Z = 0.001$ with the left-hand plot having $f_{\rm b} = 0.1$ and the right-hand plot having $f_{\rm b} = 0.5$. Concentrations are $r_{\rm t}/r_{\rm h} = 37$ (solid), $r_{\rm t}/r_{\rm h} = 75$ (dotted) and $r_{\rm t}/r_{\rm h} = 180$ (dashed). 9 $t_{\rm rh}$ is the dynamical age of the simulation with $r_{\rm t}/r_{\rm h} = 37$ after $1T_{\rm H}$. The simulations with $r_{\rm t}/r_{\rm h} = 21$ are not shown since they do not reach 9 $t_{\rm rh}$ within $1T_{\rm H}$ and have too few BH–BHs at 3 $t_{\rm rh}$ for interesting statistics. Each bin is averaged over all 10 independent realizations.

The presence of eccentricity in a binary can vastly improve its prospect for GW detection. Peters & Mathews (1963) and Peters (1964) have shown that with increasing eccentricity GWs are preferentially emitted at higher harmonics of the orbital frequency. This can enhance the power emitted in GWs by a factor of 10^2 or more for binaries with $e > 0.8$ and reduce $t_{\rm in}$ by a similar factor. This enhances the chance of a relativistic merger within $1T_{\rm H}$. Emission at higher orbital harmonics produces GWs with higher frequencies that would be produced by identical binaries with circular orbits. Thus eccentricity can bring long-period binaries into the LISA band. In Fig. 8 we show the eccentricity of our BH–BH binaries as a function of period. It must be noted that these eccentricities are produced randomly upon creation of a binary, do not experience self-consistent dynamical evolution during interactions and are subject to circularization in the course of binary evolution in BSE. Interactions tend to increase the eccentricity of binaries and thus the eccentricities produced by our simulations should be taken as lower limits. Even with this caveat, Fig. 8 shows that there are a wide range of eccentricities for any given period.

Since some of our binaries are eccentric and since this eccentricity can significantly reduce the inspiral time-scale of the binary, we use equation (13) to estimate the inspiral time-scale of all BH–BH binaries in our simulations. The result is given in Fig. 9 the trends of which simply reflect the period distribution in Fig. 7. It is apparent that even with eccentricity included there are very few binaries with an inspiral time-scale shorter than $1T_{\rm H}$. For the few BH–BH binaries with $t_{\rm insp} < 10^5$ Myr the dynamics play a destructive role. Fig. 10 shows the time-scale for dynamical disruption or ejection of BH–BH binaries, $t_{\rm dis}$. It is apparent that the average $t_{\rm dis}$ for BH–BH binaries is very short, between 1 and 100 Myr in most cases, and is shorter in the more concentrated clusters due to the higher interaction rate. There is little between the distributions in Figs 9 and 10 and $t_{\rm in} > t_{\rm dis}$ in almost all cases. Indeed in none of our simulations do we find any BH–BH binary mergers. Some of the eccentric, short-period binaries in our simulations may, however, have a chance of appearing in the LISA band and we will turn to this possibility in Section 5.2.

Although we find no mergers within the clusters, the simulations eject hard binaries. Fig. 11 shows the distribution of binding energies for escaping BH–BH binaries. $E_{\rm bind}$ is, on average, much higher for the escapers than for the system as a whole. This is because the most tightly bound binaries tend to receive the highest recoil velocities in few-body encounters and are thus the most likely to be ejected from the system. Therefore the most promising merger candidates are the least likely to remain in the cluster. The distribution in Fig. 11 compares favourably with the results from O'Leary et al. (2006) (their fig. 6) which were derived based on explicit few-body integration. This agreement increases our confidence that both the few-body encounters and the dense core dynamics are being reproduced successfully in our code.

5 GRAVITATIONAL WAVE DETECTION

In this section we consider the prospects for GW detection in both the ground- and space-based frequency bands.

5.1 Ground-based sources

Because of the long inspiral times and short disruption times shown in Figs 9 and 10 we find no compact mergers in any of our simulations. Thus the BH–BH binary destruction rate within the cluster dominates the creation rate and all BH–BH binaries are either ejected or disrupted before they have a chance to inspiral and merge. We therefore predict that GCs as objects will not contribute significantly to the ground-based GW detector signal. Many of the escapers produced by GC dynamics should, however, merge in the galactic field within a Hubble time and thus may contribute to the detection rate. We save analysis of these sources for a follow-up

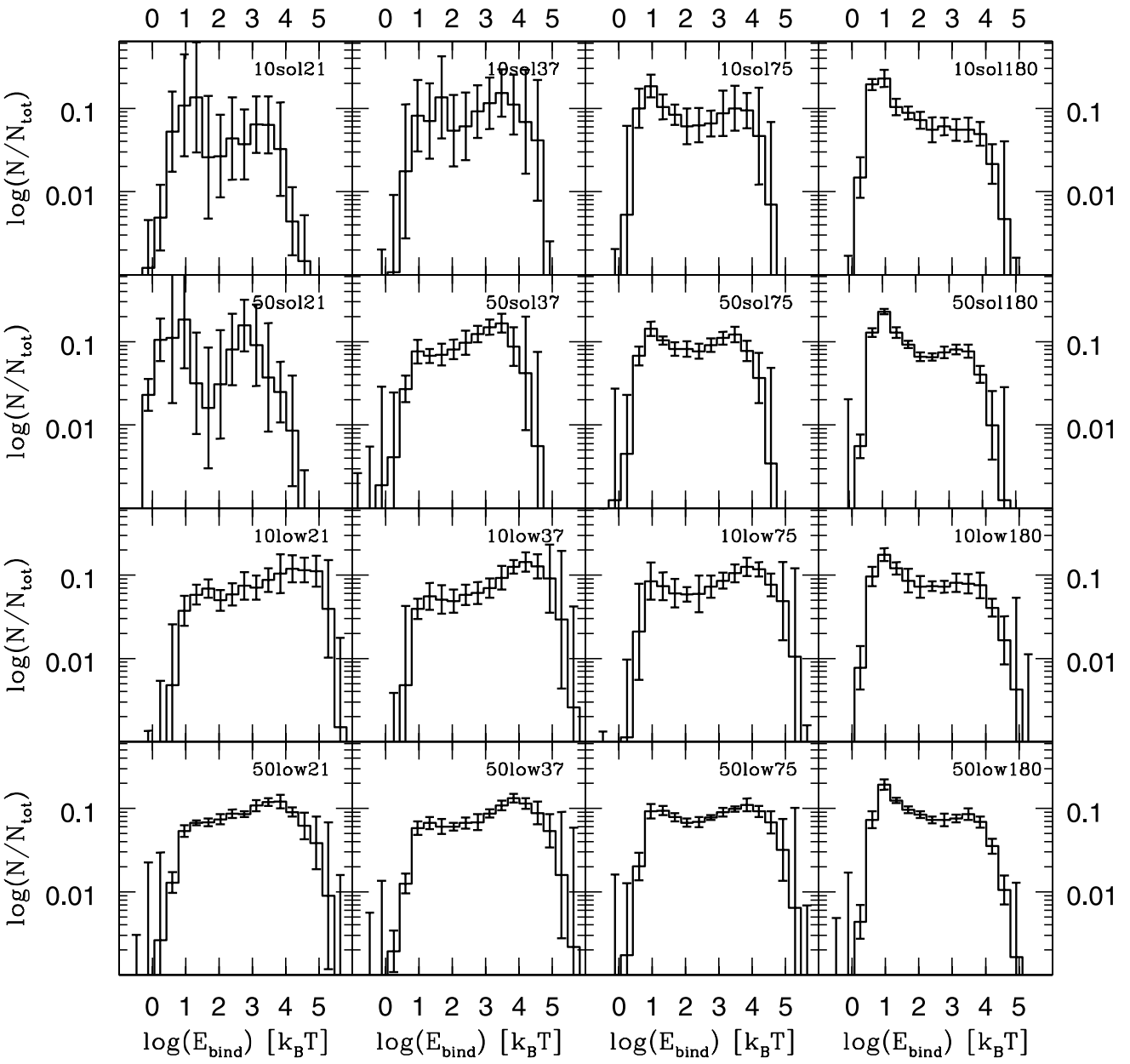

Figure 6. Cumulative binding energy distribution of BH–BH binaries up to $1T_{\rm H}$ binned uniformly in log space. Each bin is averaged over all 10 independent realizations and the error bars give the rms scatter. Energies are in units of the thermal energy of the core of the cluster.

paper and concentrate instead on the very interesting LISA sources that we find within our simulations.

5.2 LISA sources

In order to study potential LISA sources from these simulations, we consider only those binaries present in the cluster simulations at ages between 10 and 14 Gyr. This is covers the age distribution of GCs in the Milky Way and stellar mass inspirals will not be strong enough GW sources to be observed beyond the galaxy. Advanced LIGO will be able to detect BH–BH inspirals out to moderate redshifts and for these predictions we will have to take the earlier stages of cluster evolution and the possibility of younger GCs in other galaxies into account. Of these Milky Way binaries, we further restrict them to have a combination of orbital periods and eccentricities such that the harmonic with peak power lies within the LISA sensitivity band. We estimate the frequency of this harmonic by approximating the orbit at periastron ($a(1-e)$) with a circular orbit of radius $r = a(1-e)$. The frequency of this circular orbit is then proportional to $(1-e)^{-1.5}$. However, since the orbital speed of the eccentric binary at periapsis is higher than that of a circular binary, the dominant frequency of the GW burst will be somewhat higher than the circular frequency. For a parabolic encounter, this speed difference is $\sqrt{2}$, and so the harmonic with peak power is estimated to be

$$n_{\rm max} \simeq \sqrt{\frac{2}{(1-e)^3}}. \tag{14}$$

With this age and frequency/eccentricity restriction, we find that 33 simulations have potential LISA sources. All but one of these has only one potential LISA source at any time during the 10 to

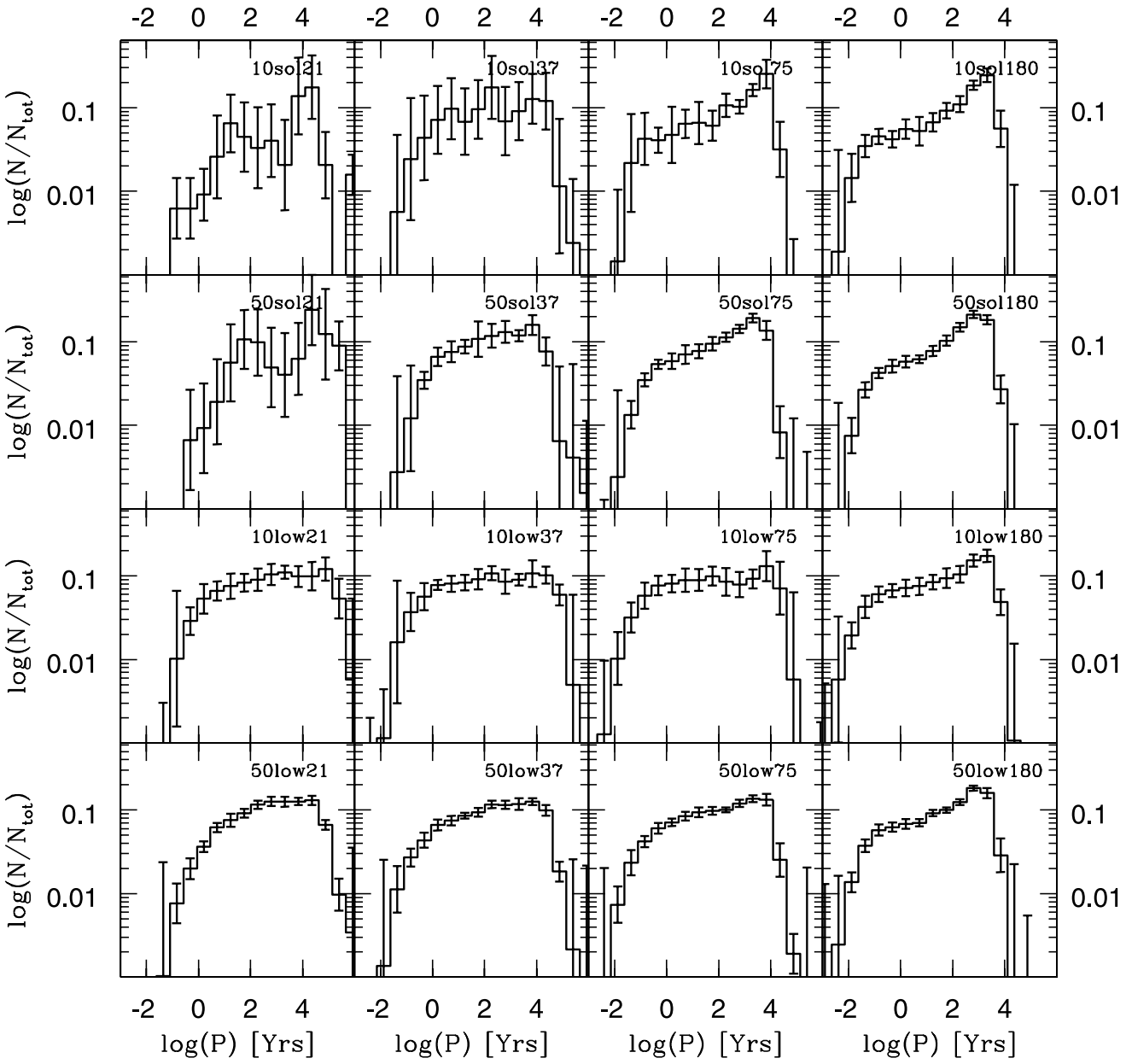

Figure 7. Cumulative period distribution of BH–BH binaries up to $1T_{\rm H}$ binned uniformly in log space. Each bin is averaged over all 10 independent realizations and the error bars give the rms scatter.

14 Gyr under consideration. The one exception (a realization of the 50low37 model) has two potential LISA sources during the age span of 10.6 to 11.6 Gyr. Six of these simulations had binaries with $e < 0.9$, with one of these having $e<0.7$. Although there are 34 potential LISA sources in these simulations, we need to determine if these BH–BH binaries will have sufficient strength to be detected by LISA. This is done by calculating the signal-to-noise ratio using

$$\rho^2 = 4 \int_0^\infty \frac{\left|\tilde{h}(f)\right|^2}{S_{\rm n}(f)}\,{\rm d}f, \tag{15}$$

where $\tilde{h}(f)$ is the Fourier transform of the response of LISA to the GW and $S_{\rm n}(f)$ is the power spectral density of the expected noise in LISA. We include both instrument noise and an estimate of the Galactic WD binary foreground from Ruiter et al. (2007).

We determine the response, $h(t)$, by placing 10 realizations of each binary in Galactic GCs that are within 5 kpc of the Earth. The properties of these clusters are obtained from Harris (1996), and are shown in Table 4. Each realization is given a sky location within the GC and then assigned random orientations and initial orbital phases. The barycentred waveform is determined using the harmonic expansion of Pierro et al. (2001) carried out to the $n \sim 1300$ harmonic. The response of LISA is calculated using the long wavelength approximation as described in Cutler (1998) for 1 yr of observation.

Setting a detection threshold of $\rho \geq 7$ in a single interferometer (which corresponds to a combined $\rho \geq 10$ in two channels of the LISA data stream) we find potentially detectable binaries in three realizations of simulation 50low37 and one realization of simulation 50sol75. The properties of these binaries are shown in Table 5. The notable features of these binaries are that they are highly eccentric.

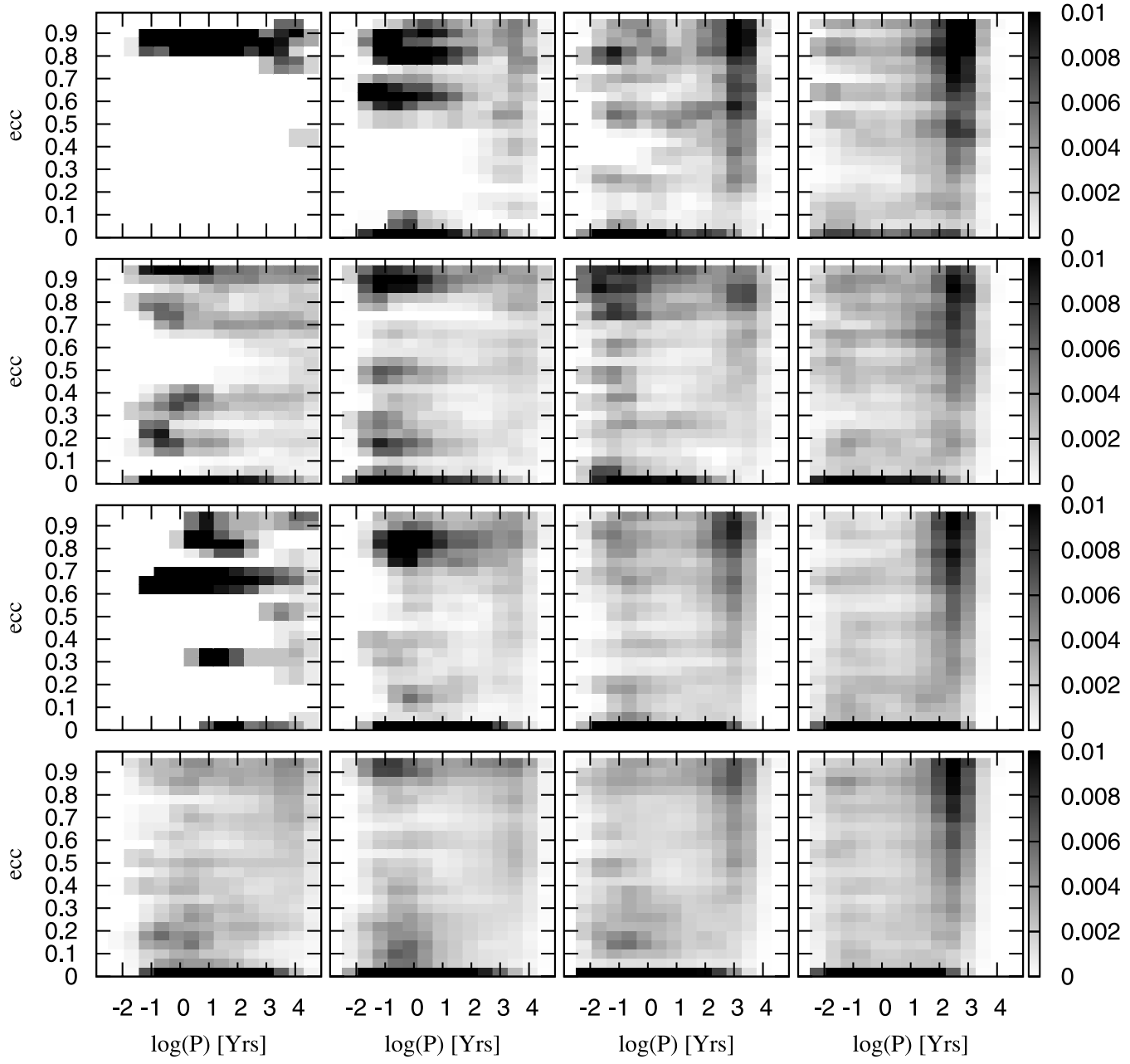

Figure 8. The eccentricity as a function of period for all BH–BH binaries at all times in all simulations. From top to bottom: $f_b = 0.1$ and $Z = 0.02$, $f_b = 0.5$ and $Z = 0.02$, $f_b = 0.1$ and $Z = 0.001$ and $f_b = 0.5$ and $Z = 0.001$. Form left to right: $r_t/r_h = 21,\ 37,\ 75$ and 180.

The long-period binary from realization nine of simulation 50low37 is only visible from a few orientations in the nearby GC NGC 6121, while the binaries in the other realizations of simulations 50low37 and 50sol75 are visible in all of the GCs chosen. The spectra of the binaries in realizations nine and four for simulation 50low37 from NGC 6121 are shown in Fig. 12 along with an estimate of the combined instrument and Galactic WD binary confusion noise. It is also interesting to note that there is a preference for high primordial binary fractions, but otherwise there is no clear dependence on cluster parameters for these sources. It must again be noted that these eccentricities are not self-consistently produced by few-body calculations and must be interpreted with caution. Furthermore, the simulations indicate at most two binaries per GC with the potential for detection by LISA and the bulk of the simulations result in no detectable systems. Consequently it is difficult to make any firm predictions about the likelihood of detection of BH–BH systems in the Galactic GC system with LISA. None the less, if we assume that high binary fractions are common in GCs and that the initial concentrations are $r_t/r_h = 37$, then roughly 30 per cent of nearby GCs may house a detectable binary.

6 DISCUSSION

Although we produce no compact binary mergers within our simulations, we can still compare our dynamics to O'Leary et al. (2006) and Sadowski et al. (2008). As described in Section 1, O'Leary et al. (2006) assume that the BHs are sufficiently mass segregated

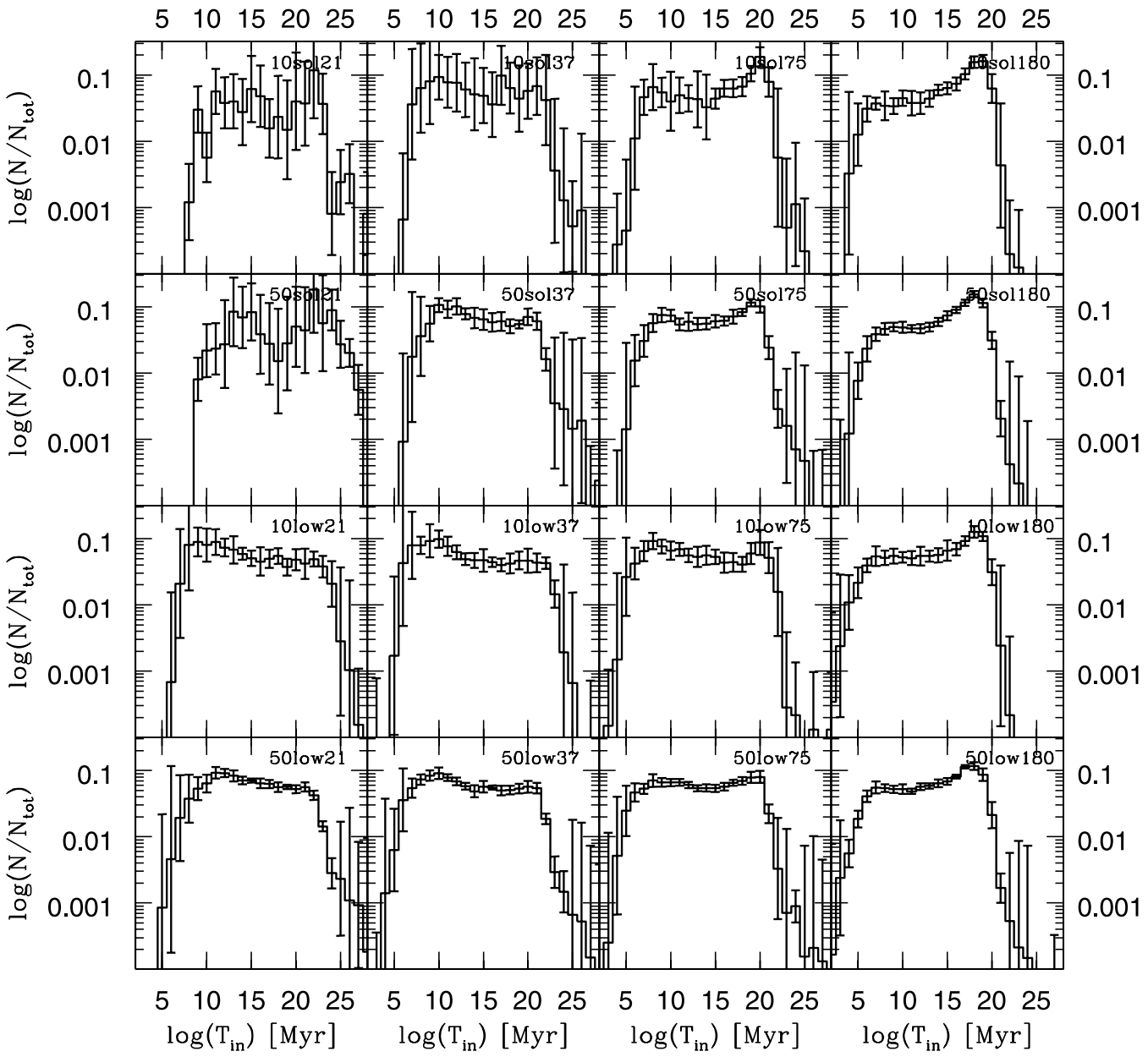

Figure 9. Cumulative distribution of BH–BH binary GW inspiral time-scale up to $1T_{\rm H}$ binned uniformly in log space. Each bin is averaged over all 10 independent realizations and the error bars give the rms scatter.

that they form a decoupled subsystem at the centre of the cluster and interact only with themselves. By contrast Sadowski et al. (2008) assume that the BHs always remain in equilibrium with the rest of the cluster and, since they do not become centrally concentrated, remain at much lower density than in the mass-segregated case. Therefore the BH–BH binaries in the O'Leary et al. (2006) simulations frequently interact with each other whereas the BH–BH binaries in Sadowski et al. (2008) do not. This means that the BH–BH binary formation rate reported in O'Leary et al. (2006) is much higher than that reported in Sadowski et al. (2008). However, since the BH–BH binaries are the only objects in the system massive enough to disrupt and eject other BH–BH binaries, the BH–BH binaries in the O'Leary et al. (2006) simulations are much more likely to be disrupted than the binaries in the Sadowski et al. (2008) simulations. In practice the lower disruption rate wins and Sadowski et al. (2008) produces a larger and more constant rate of BH–BH mergers than does O'Leary et al. (2006). Therefore, O'Leary et al. (2006) provide a lower limit on GW detection rates and Sadowski et al. (2008) provide an upper limit.

Our simulations, including full global dynamics, suggest that the O'Leary et al. (2006) approximation is more accurate. Fig. 3 shows that the BHs in our simulations mass segregate swiftly and that BH–BH binaries form in the centre of the cluster. The short dynamical disruption time-scales in Fig. 10 imply that the BH–BH binaries interact strongly with each other and are swiftly destroyed. The binding energy distribution of escapers in Fig. 11 shows that hard binaries are preferentially ejected from the cluster, suggesting a dynamical ejection scenario. Finally the time-dependant number of BH–BH binaries per Gyr reported in Fig. 2, particularly for the dense clusters, is more consistent with the time-dependent merger

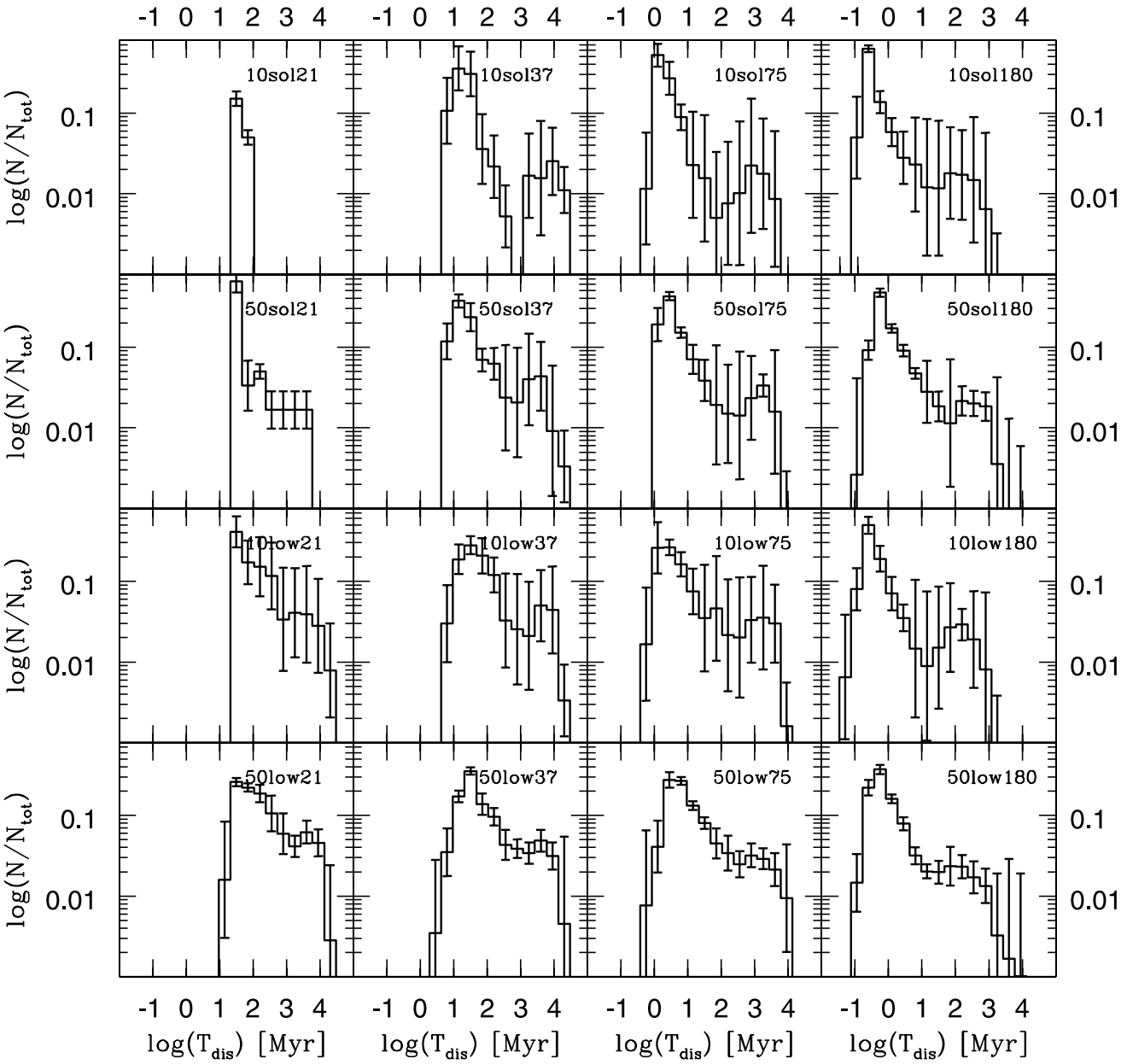

Figure 10. Cumulative distribution of BH–BH binary dynamical disruption time-scale up to $1T_{\rm H}$ binned uniformly in log space. Each bin is averaged over all 10 independent realizations and the error bars give the rms scatter.

rates of O'Leary et al. (2006) than the constant merger rate found in Sadowski et al. (2008).

A major difference between our results and those of both O'Leary et al. (2006) and Sadowski et al. (2008) is that we find no BH–BH mergers within our simulated clusters. O'Leary et al. (2006) find at least 30 per cent of their mergers occur within the clusters and Sadowski et al. (2008) find 90 per cent. The difference between O'Leary et al. (2006) and Sadowski et al. (2008) is due to the larger number of interactions and hence the larger number of ejections in the O'Leary et al. (2006) simulations. Our lack of mergers within the clusters is a result our high interaction rates but is also affected by the more approximate treatment of few-body interactions in our Monte Carlo code. In particular our binary–binary interaction prescriptions follow those of Stodółkiewicz (1986) and in these prescriptions 88 per cent of all interactions result in the disruption of the softer binary. This works well for normal binary–binary interactions but may overpredict the disruption rate in interactions between two hard BH–BH binaries. In reality more of these binaries should probably survive and be hardened by the interaction. The prescriptions also gives $0.516(E_{\rm b1} + E_{\rm b2})$, where $E_{\rm b1,2}$ are the binding energies of the two binaries, as increased binding energy to the hard binary and distributes the same amount as kinetic energy between the centres of mass after the interaction. In general this produces the correct hardening of the surviving binary (compare the energy distribution in Fig. 11 to fig. 6 in O'Leary et al. 2006) but could well produce recoil velocities and hence escape rates that are systematically too high. Furthermore, these prescriptions allow neither mergers during the interaction nor long-lived hierarchical triples. The combination of all these effects means that the number of mergers within our clusters is almost certainly too low.

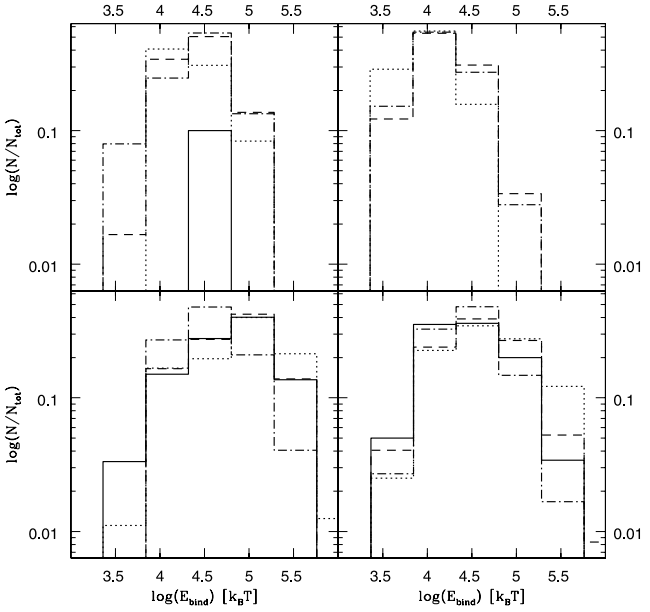

Figure 11. The binding energy of BH–BH binary escapers binned uniformly in log space. The top row shows the $Z = 0.02$ simulations and the bottom the $Z = 0.001$ ones. In the right-hand column are simulations with $f_b = 0.1$ and in the left simulations with $f_b = 0.5$. Concentrations are $r_t/r_h = 21$ (solid), $r_t/r_h = 37$ (dotted), $r_t/r_h = 75$ (dashed) and $r_t/r_h = 180$ (dot–dashed). Each bin is averaged over all 10 independent realizations.

Table 4. Celestial coordinates and distances for the 16 GCs within 5 kpc of Earth.

Name	RA			Dec.			Dist
	h	m	s	°	′	″	(kpc)
NGC 104	00	24	05.2	−72	04	51	4.5
E3	09	20	59.3	−77	16	57	4.3
NGC 3201	10	17	36.8	−46	24	40	5.0
NGC 6121	16	23	35.5	−26	31	31	2.2
NGC 6218	16	47	14.5	−01	56	52	4.9
NGC 6254	16	57	08.9	−04	05	58	4.4
NGC 6366	17	27	44.3	−05	04	36	3.6
NGC 6397	17	40	41.3	−53	40	25	2.3
NGC 6540	18	06	08.6	−27	45	55	3.7
NGC 6544	18	07	20.6	−24	59	51	2.7
2MSGC01	18	08	21.8	−19	49	47	3.6
2MSGC02	18	09	36.5	−20	46	44	4.0
Ter12	18	12	15.8	−22	44	31	4.8
NGC 6656	18	36	24.2	−23	54	12	3.2
NGC 6752	19	10	52.0	−59	59	05	4.0
NGC 6838	19	53	46.1	18	46	42	4.0

Our simulations represent the first quantitative study of stellar-mass BH–BH binaries as LISA sources within star clusters. We can compare our results to the number of stellar-mass sources predicted in the Galactic field population by Belczynski et al. (2008) and quoted in Section 1. When normalized to the total mass in their simulations, Belczynski et al. (2008) find, in the case where mergers on the Hertzsprung gap are not allowed, 2×10^{-5} resolvable LISA sources in the Milky Way per $10^5\,M_\odot$, 1×10^{-5} of which per $10^5\,M_\odot$ are BH–BH. In the case where mergers during the Hertzsprung gap are allowed they find 4×10^{-6} per $10^5\,M_\odot$, of which none is BH–BH. Assuming all four of the sources in our simulations are resolved at the current time this yields 6×10^{-3} detections per $10^5\,M_\odot$ from our simulations, all BH–BH. This rate depends on the parameters of the individual binaries but has no clear dependence on the cluster parameters. All sources are highly eccentric, indicating that eccentric stellar mass sources may be present in the LISA band. Many of our escaping binaries also have periods of a day or less and will almost certainly appear in the LISA band at some point. This does, however, place a limitation on the interpretation of the results of Belczynski et al. (2008). In their model the presence of stellar-mass BH–BH binaries in the LISA band would indicate that mergers in the Hertzsprung gap are rare whereas our results show that even if mergers on the Hertzsprung gap are common, BH–BH binaries could still exist in the LISA band due to dynamical processes in star clusters. However, the BH–BH binaries generated through dynamical processes will be associated with individual GCs if they are retained, or in the halo if they have been ejected. This is a distinct population from the disc population of binaries found in Belczynski et al. (2008).

Finally we note in passing that although we have analysed our simulations in terms of compact binaries they are in no way limited to such studies. Stellar evolution is calculated for all stars in the cluster and thus our simulations represent a complete star cluster populations synthesis study based on the stellar evolution tracks of Hurley et al. (2000, 2002). We hope to make the full results of

Table 5. Properties of the detectable LISA sources from these simulations. If the orbital period decreases during the observation time, a range is given.

Simulation	Age (Gyr)	M_1 ($M_\odot$)	M_2 ($M_\odot$)	P_{orb} ($\times 10^3$ s)	e
50low37.4	<10.2	20.5	25.9	920–490	0.988
50low37.9	>12.5	11.1	16.8	1190	0.986
50low37.10	>11.6	28.4	14.3	215	0.933
50sol75	<10.1	10.8	8.5	479–257	0.998

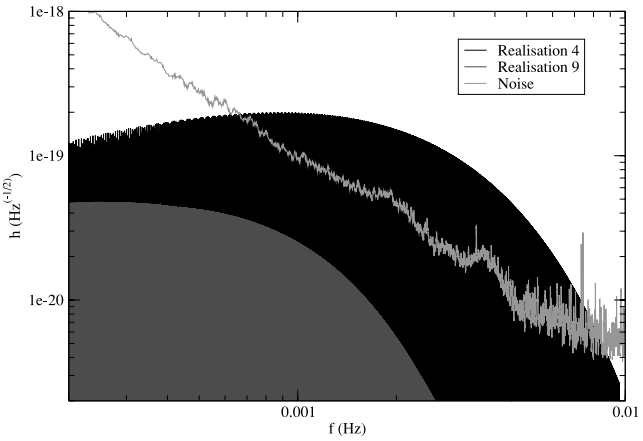

Figure 12. GW spectra of two BH–BH binaries from simulation 50low37 compared with combined instrumental and Galactic WD binary confusion noise. The weak signal is from realization 9 and the strong signal is from realization 4. Here, we have calculated the waveform out to the $n \sim 5000$ harmonic to show the full spectrum of the binaries. For the calculation of the signal-to-noise ratio, both signals are cut-off at a frequencies around 2 mHz because we only use harmonics below $n = 1300$. Note that the true signal-to-noise ratio is likely higher than we have calculated.

our simulations publicly available in the near future and encourage anyone who is interested in such data to contact the authors.

7 CONCLUSIONS

We have studied the dynamics of the BH population in star clusters with a self-consistent Monte Carlo treatment of the global dynamics and full stellar and binary evolution. We confirm the predictions of Sigurdsson & Phinney (1993) that BH–BH, but not NS–NS or NS–BH, binaries are produced efficiently in star clusters by dynamical interactions. We find that the BHs are mass segregated and interact strongly with each other, confirming the more approximate models of O'Leary et al. (2006). We find no BH–BH mergers within the clusters we simulate but many hard BH–BH escapers that will merge in the galactic field within a Hubble time. Detection rates for both ground- and space-based detectors will be calculated and presented in a future paper. We find that our simulations produce potential LISA sources that, while rare, will be highly eccentric and may still represent a significant enhancement to the galactic field population. We will certainly produce more detections when the escapers are included. We conclude that star clusters produce BH–BH binaries efficiently and must be taken into account when considering detection rates for both ground- and space-based detectors.

ACKNOWLEDGMENTS

JMBD would like to thank the International Max-Planck Research School for Astronomy and Cosmic Physics at the University of Heidelberg (IMPRS-HD) for providing funding for his PhD. The simulations have been carried out at the High Performance Computing Center Stuttgart (HLRS) using the resources of Baden-Württemberg grid (bwgrid) through the German Astrogrid-D and D-Grid projects. MJB acknowledges the support of NASA Grant NNX08AB74G and the Center for Gravitational Wave Astronomy, supported by NSF award #0734800. MG was supported by Polish Ministry of Science and Higher Education through the grant 92/N.ASTROSIM/2008/0 and N N203 380036. RS thanks the Deutsches Zentrum für Luft- und Raumfahrt (DLR) for support within the LISA Germany project.

REFERENCES

Abbott B. et al. (LIGO Scientific Collaboration), 2005, Phys. Rev. D, 72, 082001
Abbott B. et al. (LIGO Scientific Collaboration), 2006, Phys. Rev. D, 73, 062001
Baumgardt H., 2001, MNRAS, 325, 1323
Belcyznski K., Kalogera V., Bulik T., 2002, ApJ, 572, 407
Belczynski K., Sadowski S., Rasio F. A., Bulik T., 2006, ApJ, 650, 303
Belczynski K., Taam R. E., Kalogera V., Rasio F. A., Bulik T., 2007, ApJ, 662, 504
Belczynski K., Benacquista M., Bulik T., 2008, ApJ, submitted (arXiv:0811.1602v2)
Benacquista M., 2001, Classical Quantum Gravity, 19, 1297
Cutler C., 1998, Phys. Rev. D, 57, 7089
Evans C. R., Iben I., Smarr L., 1987, ApJ, 323, 129
Fregeau J. M., Rasio F. A., 2007, ApJ, 658, 1047
Giersz M., 1998, MNRAS, 298, 1239
Giersz M., 2001, MNRAS, 324, 218
Giersz M., 2006, MNRAS, 371, 484
Giersz M., Heggie D. C., 1994, MNRAS, 268, 257
Giersz M., Heggie D. C., 2008, MNRAS, 389, 1858
Giersz M., Heggie D. C., 2009, MNRAS, 395, 1173
Giersz M., Spurzem R., 2003, MNRAS, 343, 781
Giersz M., Heggie D. C., Hurley J. R., 2008, MNRAS, 388, 429
Gültekin K., Miller M. C., Hamilton D. P., 2004, ApJ, 616, 221
Hansen B. M. S., Phinney E. S., 1997, MNRAS, 291, 569
Harris W. E., 1996, AJ, 112, 1487
Harris W. E., Whitmore B. C., Karakla D., Okoń W., Baum W. A., Hanes D. A., 2006, ApJ, 636, 90
Heggie D. C., 1975, MNRAS, 173, 729
Heggie D. C., Giersz M., 2009, MNRAS, 397, 46
Heggie D. C., Hut P., McMillan S. L. W., 1996, ApJ, 467, 359
Hénon M., 1971, Ap&SS, 13, 284
Hils D., Bender P. L., Webbink R. F., 1990, ApJ, 360, 75
Hurley J. R., Pols O. R., Tout C. A., 2000, MNRAS, 315, 543
Hurley J. R., Tout C. A., Pols O. R., 2002, MNRAS, 329, 897
Ivanova N., Heinke C. O., Rasio F. A., Belczynski K., Fregeau J. M., 2008, MNRAS, 386, 553
Kalogera V., Narayan R., Spergel D. N., Taylor J. H., 2001, ApJ, 556, 340
Khalisi E., Amaro-Seoane P., Spurzem R., 2007, MNRAS, 374, 703
Kroupa P., 1995, MNRAS, 277, 1507
Kroupa P., Tout C. A., Gilmore G., 1993, MNRAS, 251, 293
Lorimer D., 2005, Living Rev. Relativ., 8, 7
Lyne A. G., Lorimer D. R., 1994, Nat, 369, 127
Mikkola S., 1984, MNRAS, 208, 75
Nelemans G., Yungelson L., Portegies Zwart S. F., 2001, A&A, 375, 890
O'Leary R. M., Rasio F. A., Fegeau J. M., Ivanova N., O'Shaughnessy R., 2006, ApJ, 637, 937
Peters P. C., 1964, Phys. Rev., 136, 1224
Peters P. C., Mathews J., 1963, Phys. Rev., 131, 435
Pierro V., Pinto I., Spallicci A., Laserra E., Recano F., 2001, MNRAS, 325, 358
Portegies Zwart S. F., McMillan S. L. W., 2000, ApJ, 528, 17
Portegies Zwart S. F., Hut P., McMillan S. L. W., Makino J., 2004, MNRAS, 351, 473
Ruiter A., Belczynski K., Benacquista M., Larson S., Williams G., 2007, ApJ, submitted (arXiv:0705.3272v3)
Sadowski A., Belczynski K., Bulik T., Ivanova I., Rasio F. A., O'Shaughnessy R., 2008, ApJ, 676, 1162
Sigurdsson S., Phinney E. S., 1993, ApJ, 415, 631
Spitzer L., 1987, Dynamical Evolution of Globular Clusters. Princeton Univ. Press, Princeton, NJ
Stodółkiewicz J. S., 1982, Acta Astron., 32, 63
Stodółkiewicz J. S., 1986, Acta Astron., 36, 19
Timpano S. E., Rubbo L. J., Cornish N. J., 2006, Phys. Rev. D, 73, 122001
Watters W. A., Joshi K. J., Rasio F. A., 2000, ApJ, 539, 331

This paper has been typeset from a TEX/LATEX file prepared by the author.